Title: Transported scalar PDF calculations of a swirling bluff body flame ('SM1') with a Reaction Diffusion Manifold

Authors: R. De Meester, B. Naud, U. Maas, B. Merci

In: Combustion and Flame, Volume 159, Issue 7, Pages 2415-2429

Optional: http://dx.doi.org/10.1016/j.combustflame.2012.01.026

Transported scalar PDF calculations of a swirling bluff body flame ('SM1') with a Reaction Diffusion Manifold

R. De Meester[a], B. Naud[b], U. Maas[c], B. Merci[a]

[a] *Department of Mechanics of Flow, Heat and Combustion, Ghent University, St-Pietersnieuwstraat 41, 9000 Gent, Belgium, reni.demeester@ugent.be*
[b] *Modeling and Numerical Simulation Group, Energy Department, Ciemat, Avda. Complutense 22, 28040 Madrid, Spain, bertrand.naud@ciemat.es*
[c] *Institute for Technical Thermodynamics, Karlsruhe University (TH), Kaiserstraße 12, 76128 Karlsruhe, Germany, umaas@itt.uni-karlsruhe.de*

Abstract

The modeling of a reacting swirling flow behind a bluff-body burner (SM1) in the framework of RANS and transported scalar PDF is presented. The EMST mixing model is applied and the composition space is reduced to mixture fraction (Z) and a progress variable (CO_2 mass fraction, Y_{CO_2}) by means of a Reaction Diffusion Manifold (REDIM). With an ad hoc adjustment of the turbulent Schmidt number, the mean flow and mixing fields obtained are comparable to LES results from the literature. The REDIM reduction of the composition space to (Z, Y_{CO_2}) is discussed and its validity for the present swirling flame is first considered by an a priori comparison with experimental data. The (Z, Y_{CO_2})-scatter plots from the transported PDF calculation show the capacity to reproduce the mixing between fresh air and hot products in the recirculation zone above the bluff-body. However, too little scatter is observed. The study of tracer trajectories helps to better understand the capacities and limitations of the modeling approach. Zones where mixing competes with reaction can be identified, and coincide with the highly rotating collar region where local extinction is expected to take place. However, in our modeling, the competition between mixing and reaction is not enough to lead to local extinction. An important modeling deficiency is claimed to be the use of a mean time scale in the EMST mixing model, which limits the possibilities to model high scalar dissipation rate events.

Keywords: flamelet, REDIM, progress variable, PDF, swirling flame

1. Introduction

Swirl-stabilized turbulent flames are important for many industrial applications, because the swirling motion creates recirculation zones which enhance mixing and stabilize the flame. This leads to better combustion efficiency and less pollutant formation. However, swirl flames are not yet fully understood. One of the complex phenomena concerns vortex breakdown leading to flow instability, i.e. a precessing vortex core and periodically expanding/shrinking recirculation zone. Several modeling approaches have been used to simulate these complex flows. The unsteady 3D effects are in principle better handled by LES than RANS, but LES calculations have a higher computational cost. Therefore, we consider it still useful to study hybrid RANS/PDF (probability density function) calculations, in particular for cases where there is no strong influence from a precessing vortex core.

Besides flow field complexity, local extinction is also important, as it leads to e.g. incomplete combustion and therefore more pollutants. Physically, extinction in laminar non-premixed flames occurs due to local high gradients, resulting in excessive local heat (and mass) transfer, which cannot be sustained by local heat production from chemical reactions [1]. It is characterized by the local Damköhler number, defined as the inverse of the product of the chemical time scale and the scalar dissipation rate. In [2] Kolmogorov scale eddies are stated to be important in the extinction of turbulent non-premixed flames with a similar physical mechanism as for laminar flames. In [3], on the other hand, extinction is said to be caused by large-scale eddies through total flame stretching, and not through small-scale flame wrinkling. There are also other mechanisms for local extinction, e.g. radical pools being swept away by a vortex [4]. Apart from experiments, also DNS studies have been done to investigate local extinction of non-premixed flames. In [5], following Lagrangian particles in the flow, it is shown that local extinction is purely due to fluctuations of the scalar dissipation rate. In [6], where DNS with one-step global reaction is performed in order to study the influence of turbulent mixing on re-ignition, local extinction is again shown to be due to fluctuations of the scalar dissipation rate, causing excessive heat loss.

In transported PDF modeling, traditional mixing models use the mean integral turbulent time scale in order to determine the mixing time scale. Moreover, in a RANS framework, the flow and mixing fields in physical space are steady and not all fluctuations in scalar dissipation rate can be expected to be captured. The PSP model [7–10], which uses one-dimensional

parametrized scalar profiles (PSPs) to model the unresolved scalar length-scales characterizing the scalar micro-mixing, can capture the fluctuations in scalar dissipation rate better, as it provides joint statistics of scalars and their scalar dissipation rate. In LES, resolved fluctuations in instantaneous flow and mixing fields result in resolved fluctuations of the scalar dissipation rate. In [11], where LES calculations with presumed PDF modeling and a flamelet generated manifold [12] are discussed, coherent structures of high scalar dissipation are seen to lead to flame stretching and local extinction.

In the present study, we investigate the swirling bluff body flame SM1 [13–17], which has been studied numerically in the past by several authors. Masri et al. [18] performed a joint velocity-scalar-frequency PDF calculation for a reacting case. James et al. [19] performed an LES/PDF calculation of two reacting cases (SM1 and SMA1) with satisfactory results. Unfortunately no detailed study of turbulence-chemistry interaction is reported. LES results of non-reacting and reacting cases have been presented with flamelet chemistry in [20–23] and with FGM chemistry in [24]. A comparable quality of flow and mixing field results is obtained here with axisymmetric steady RANS calculations with a non-linear k-ϵ model [25]. The obvious advantage of this approach is that transported (scalar) PDF simulations can be performed within reasonable computing time, in order to study turbulence-chemistry interaction.

For chemical reaction, a pre-calculated chemistry table is used. We adopt the Reaction Diffusion Manifold (REDIM) [26] approach, as it has already been used for calculations of non-swirling bluff-body flames [27, 28]. In the latter, the combination of REDIM with EMST mixing model [29] led to reasonable results, but scatter in Y_{CO_2} space was clearly under-estimated. This was not attributed to the use of REDIM as reduced chemistry, but to the localness property of EMST leading to too little local extinction. In the present paper, we discuss results with similar model settings, but for a swirling flame. Moreover the trajectories in physical and composition space of computational particles are studied in detail. This proves to be useful in order to correlate positions in composition space and in physical space. It also permits to focus on the distinction between mixing and extinction, and to discuss the limitations of the modeling in a more precise manner — for instance to better formulate the limitation of EMST instead of generally referring to its 'localness in composition space'.

2. Test case description and modeling framework

2.1. Sydney swirling flame SM1

Figure 1 depicts the burner. The bluff body (50mm diameter) contains the central fuel jet (3.6mm diameter). Swirling air is provided through a 5mm wide annulus surrounding the bluff-body. The swirl component is created by three tangential ports. The burner is placed inside a wind tunnel with square cross section. A wide range of testing conditions has been examined experimentally [13–17]. All cases are characterized by: the bulk axial velocity of the central jet (U_j), the bulk axial and tangential velocities of the swirling air annulus (U_s and W_s) and the bulk axial velocity of the co-flow of the wind tunnel (U_e).

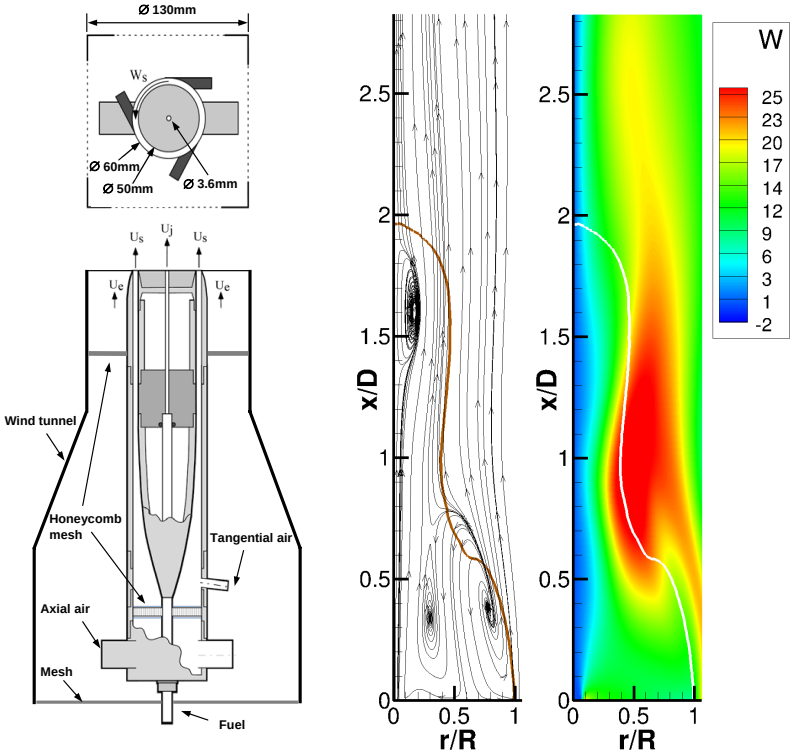

Figure 1: Sydney Swirl Burner (adapted from [30]) and stream lines and contours of tangential velocity in an axisymmetric slice of a transported PDF calculation with EMST and REDIM. Brown and white lines: stoichiometric mixture fraction isocontour.

We consider flame SM1 only, because for this flame the precessing vortex core is the weakest. This is important since we consider here a steady RANS modeling framework. In the experiments [17], velocity measurements were performed with CNG, while CH_4 was used for the composition measurements. No physical changes in the flow field are reported. We use CH_4 as fuel in the simulations. The stoichiometric mixture fraction is $Z_{\mathrm{st}} = 0.054$. The flow parameters are summarized in Table 1 with the swirl number geometrically defined as $S_g = W_s/U_s$. The flow field of SM1 contains two recirculation zones: one close to (and caused by) the bluff body and one further downstream near the central axis (caused by vortex breakdown). The simulation results (Figure 1, right) reproduce the qualitative experimental finding that the recirculation zones are separated by a region of high shear stress which coincides with a highly rotating collar. In [17], local extinction is believed to occur in this region of high shear stress between the two recirculation zones, while the hot, re-circulated combustion products from the second recirculation zone are believed to cause re-ignition.

Table 1: Flow parameters of SM1

Case	Fuel	U_e (m/s)	U_j (m/s)	U_s (m/s)	W_s (m/s)	S_g (-)
SM1	CNG/CH_4	20	32.7	38.2	19.1	0.5

2.2. Turbulence-chemistry interaction in RANS modeling framework

The non-linear k-ϵ turbulence model of [25] is used, as it takes into account the effect of streamline curvature and rotation on turbulence.

In order to deal with turbulence-chemistry interaction, a transported scalar PDF approach is used. In the transported scalar PDF approach, the transport equation is modeled and solved for the mass density function $\mathcal{F}_\phi(\boldsymbol{\psi}) = \rho(\boldsymbol{\psi})\, f_\phi(\boldsymbol{\psi})$, with f_ϕ the joint scalar PDF [31], and with $\boldsymbol{\phi}$ the composition vector of independent scalars, (in this work) consisting of mixture fraction, Z, and CO_2 mass fraction, Y_{CO_2}:

$$\frac{\partial \mathcal{F}_\phi}{\partial t} + \frac{\partial \widetilde{U}_j \mathcal{F}_\phi}{\partial x_j} + \frac{\partial}{\partial \psi_\alpha}\left[S_\alpha(\boldsymbol{\psi})\, \mathcal{F}_\phi\right] \tag{1}$$
$$= \underbrace{-\frac{\partial}{\partial x_j}\left[\left\langle u_j'' \middle| \boldsymbol{\psi} \right\rangle \mathcal{F}_\phi\right]}_{\text{gradient diffusion}} \underbrace{- \frac{\partial}{\partial \psi_\alpha}\left[\frac{1}{\rho(\boldsymbol{\psi})}\left\langle -\frac{\partial J_j^\alpha}{\partial x_j} \middle| \boldsymbol{\psi} \right\rangle \mathcal{F}_\phi\right]}_{\text{mixing model}}.$$

In this general equation, S_α is the reaction source term for scalar α and $\boldsymbol{J}^\alpha$ the molecular scalar flux.

A Lagrangian particle method is used to model and solve (1) [31]. The two terms on the right hand side need to be modeled. For the first term, the effect of conditional velocity fluctuations is modeled as a turbulent diffusion flux, by using a gradient diffusion model:

$$\frac{\partial}{\partial x_j}\left[\left\langle u_j''\middle|\boldsymbol{\psi}\right\rangle\mathcal{F}_\phi\right] = -\frac{\partial}{\partial x_j}\left[\Gamma_T\frac{\partial\left(\mathcal{F}_\phi/\langle\rho\rangle\right)}{\partial x_j}\right], \tag{2}$$

where Γ_T is the turbulent diffusivity, modeled as $\Gamma_T = \mu_T/Sc_T$, with μ_T the dynamic turbulent viscosity (from the model of [25]), and with the turbulent Schmidt number Sc_T chosen to be variable depending on $\widetilde{uv}$ (see Appendix A). For the second term on the right hand side of Eq. (1), which represents the effect of molecular diffusion in the turbulent flow, we use the EMST mixing model [29] with $C_\phi = 2$.

2.3. Hybrid RANS/PDF approach

All calculations are steady axisymmetric and are performed with the same code PDFD [32], which has already successfully been applied to non-swirling Sydney bluff-body burner cases [27, 28]. In transported PDF calculations, the equations are solved using a consistent hybrid finite-volume/particle method [32]. Mean velocity $\widetilde{U}$, turbulent kinetic energy k and turbulent dissipation rate ϵ are obtained by a standard finite-volume (FV) method based on a pressure correction algorithm. The transport equations for turbulent kinetic energy (k) and turbulent dissipation rate (ϵ) solved in the FV method provide the turbulent timescale, required in the mixing model. The mean density $\langle\rho\rangle$ in the FV method is obtained from the iteration averaged mean density in the particle method (averaged over 1000 particle time steps).

For the evolution of the particles the fractional step method is used [31]. In every particle time step, the particles first mix and subsequently react. The mixing causes particle motion in 2D composition space of the independent scalars to a new position (Z^*, $Y^*_{CO_2}$). At this new position the particles react with the reaction rate for CO_2 as obtained from the REDIM table (Figure 2). As mixture fraction is conserved during the reactions, the particles move in the 1D Y_{CO_2}-space to the final position in the 2D composition space of the independent scalars (Z^*, $Y^{**}_{CO_2}$). At this final position all the dependent scalars, e.g. temperature, density and species, are retrieved from the

REDIM table. A local time-stepping algorithm, developed in the framework of statistically stationary problems [33], is applied. The number of particles per cell is 100.

An outer iteration consists of a number of FV iterations and particle time steps. We use a fixed number of particle time steps (typically 5), while the FV method is iterated until the residuals of all equations are decreasing and the global mean pressure correction is below a specified threshold (with a maximum of 1000 FV iterations per outer iteration).

2.4. Computational domain and boundary conditions

The 0.3m long computational domain starts at the burner exit. In radial direction, it is 0.15m wide. A non-uniform rectangular grid of 160×128 cells is used. Grid independence has been verified, but will not be discussed in detail. Inlet mean velocity boundary conditions are generated from separate calculations inside the burner, using the LRR-IP turbulence model [34]. The turbulent kinetic energy (k) levels obtained from the calculations inside the burner are much lower than the experimental values measured close to the burner ($x = 1.89 D_{\text{jet}}$). Therefore, we decided to upscale the k profiles from the separate calculations by multiplying with a constant factor to match the experimentally measured peak value at $x/D = 0.2$. The profiles from the separate calculations for the turbulent frequency $\omega = \epsilon/k$ were then used to deduce the ϵ profiles. In the fuel jet, $Z = 1$, whereas the air flows correspond to $Z = 0$. The mixture fraction variance is zero at the inlet.

As already observed for the non-swirling bluff-body burner [35], we verified in presumed-PDF calculations (not shown here) that the results are insensitive to the applied boundary condition at the bluff-body face (either no-slip boundary condition, with standard wall functions or free slip boundary condition). The bluff body is treated here as a free slip wall and the gradients normal to the bluff body are assumed to be zero. Symmetry conditions are applied at the symmetry axis. A convective outlet condition is used. The outer boundary of the computational domain is modeled as a free-slip wall (symmetry boundary condition), which forces the fluxes to be zero.

2.5. Particle tracking technique

A similar technique as in [36] is used to track computational particles. Tracers are randomly selected among the particles introduced into the computational domain at the inlet. Not all particles are injected simultaneously, but since the solution is statistically stationary, the time of injection is not

essential. Special measures are taken in order to cope with the particle number control algorithm ('splitting and clustering' of computational particles). When a tracer particle is split, only one of the resulting particles continues to be a tracer particle. In case of clustering where one or more tracers are involved, the particle after clustering plays the role of the tracer. Consequently, if more than one tracer is involved in the clustering, the number of tracers is reduced. In [36] clustering was disabled to avoid this.

From a statistical point of view, each computational particle is representative of one realization of the flow [31]. In one computational cell the computational particles determine together the PDF. However, one individual computational particle does not behave exactly as a fluid element. Therefore the trajectories investigated below must not be interpreted as flow paths of fluid elements. They must be interpreted in a statistical sense. The tracers also do not represent the instantaneous flame structure [36]. Nevertheless, the trajectories in physical space and composition space provide insight in a Lagrangian manner.

In [36] the evolution of the tracers was studied using axial position as surrogate for time. This is not possible for the bluff-body case, as there are several recirculation zones, resulting in a non-monotonous evolution of the axial coordinate with time. We therefore need to use 'time' or 'particle age' to describe the progress in the evolution of the tracer, when studying multiple tracers simultaneously. The 'particle age' is set to zero at the time of injection of the particle into the domain.

3. Reduced Chemistry Modeling

The Reaction Diffusion Manifold (REDIM) [26] is used in this study as tabulated chemistry model. Obviously, there are other options to reduce the calculation time for the chemistry, such as in situ adaptive tabulation (ISAT) [37] in which a chemistry table is stored on the fly. This technique has recently been applied in parallel computations [38]. Yet, pre-calculated tables based on reduced mechanisms are still more economical in global computing time. There are also other ways than REDIM to construct manifolds, e.g. FGM [12] or FPI [39], using a progress variable. It is not intended here to compare different manifold techniques. An overview of existing techniques can be found e.g. in [40].

3.1. Reaction-Diffusion Manifold (REDIM)

In a Reaction Diffusion Manifold [26], progress variables (in this work only one, namely Y_{CO_2}) are introduced as extra parameters in addition to mixture fraction, in order to consider finite-rate chemistry effects, such as low temperature chemistry and mixing of burnt and unburnt gases. REDIM can be seen as an extension of the ILDM concept [41] to incorporate the effect of coupling of reaction and diffusion processes. Contrary to ILDM, the REDIM manifold also exists in regions where the temperature is low and thus the chemistry rate is slow. Starting from a detailed reaction mechanism with a certain number of species and reactions, the REDIM concept reduces the system to a lower dimensional invariant reaction/diffusion manifold, which approximates the full system dynamics in the state space but with fewer degrees of freedom. In the construction of the REDIM, the scalar gradients in physical space $\nabla\phi_\alpha$ need to be specified [26]. For each (Z, Y_{CO_2}) value, the final REDIM therefore includes 'underlying' scalar dissipation rates $\chi^\star_\alpha$, where $\chi^\star_\alpha = 2D_\alpha \nabla\phi_\alpha . \nabla\phi_\alpha$ depends on the specified scalar gradients $\nabla\phi_\alpha$ and on the diffusion coefficient D_α (which depends on the REDIM composition). In the REDIM concept the choice of the scalar gradients $\nabla\phi_\alpha$ determining the underlying flame structure is free. In this study the gradients form laminar diffusion flamelet calculations are used, resulting in a manifold similar to FGM [12], if the generated manifolds are based on diffusion flamelets. Note, however, that the REDIM concept allows to cover the domain, where due to strain no flamelets exist (see below).

We apply the REDIM concept to reduce the Warnatz mechanism [43] for CH_4 to a 2-dimensional manifold with mass fractions Y_{N_2} and Y_{CO_2} as independent parameters. The mixture fraction is directly related to Y_{N_2} through the following relationship:

$$Z = 1 - \frac{Y_{N_2}}{Y_{N_2,0}}, \tag{3}$$

with $Y_{N_2,0}$ the N_2 mass fraction value in the co-flowing air. This definition of mixture fraction does not account for differential diffusion. Equal diffusivities for all species and unity Lewis number are assumed.

The REDIM is stored as a pre-calculated table. Figure 2 shows contours of the CO_2 reaction rate as function of mixture fraction and Y_{CO_2}.

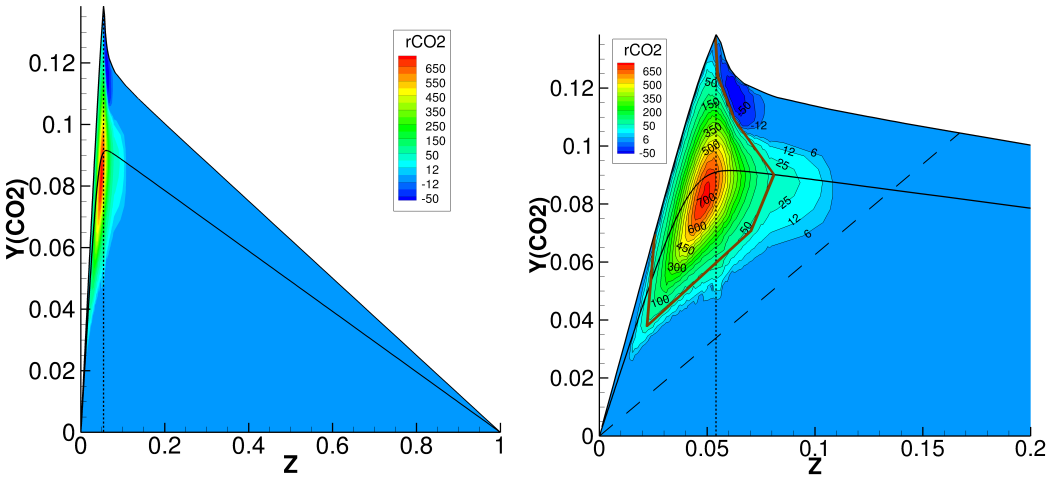

Figure 2: REDIM CO_2 reaction rate ($rCO2$). Vertical dotted line: stoichiometry ($Z_{\mathrm{st}} = 0.054$). Reference lines: 1/ steady non-premixed flamelet close to extinction, 'critical flamelet', calculated in the opposed-flow configuration with Warnatz mechanism [42, 43] (black line). 2/ reference mixing line (dashed line). 3/ approximation of iso-contour $rCO2 = 50s^{-1}$, separating zones of low and high reactivity (brown line).

3.2. Parametrization

Since mixture fraction is a conserved scalar, there is no chemical source term ($S_Z(Z, Y_{CO_2}) = 0$) and evolution in composition space in the Z-direction is only caused by mixing. The REDIM uses the progress variable approach with (in this work) Z and Y_{CO_2} as independent parameters. The latter can be seen as a non-normalized progress variable and evolution in composition space in the Y_{CO_2}-direction is caused by both mixing and reaction.

The information contained in the REDIM does not necessarily differ strongly from the information contained in a multiple flamelet, consisting of steady flamelets for a range of scalar dissipation rates. However, the essential difference is the choice of the parametrization of the data set: mixture fraction and Y_{CO_2} instead of mixture fraction and its scalar dissipation rate, $\chi = 2D\nabla Z.\nabla Z$. The influence of the parametrization can be observed when solving the flamelet equation and plotting the flamelet temperature at stoichiometry as function of χ_{st} (the scalar dissipation rate at stoichiometry). The well known S-curve is then obtained (Figure 3) [44], consisting of an upper stable burning branch, a lower stable inert mixing branch and an intermediate unstable branch representing the unstable solution of the flamelet equation. With χ as second parameter, the S-curve is projected onto the χ-

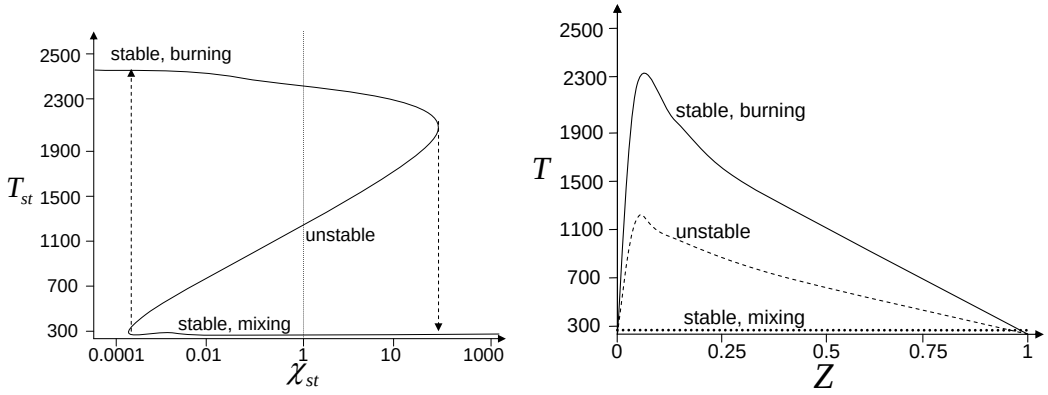

Figure 3: a/ S-Curve representing the complete solution of the flamelet equations. b/ Flamelet solutions corresponding to the 3 branches of the S-curve for $\chi = 1s^{-1}$. Adapted from [44].

axis and therefore only one branch can be represented at a time. With a progress variable, however, the S-curve is projected onto the vertical axis and the complete S-curve, including the unstable branch can be reached [44] as it evolves monotonically with the progress variable. This is discussed in several papers on the use of the flamelet/progress variable approach in LES [44–46] and most of the conclusions in those references remain valid for RANS.

With the use of a progress variable in the REDIM, also the low temperature region, which cannot be represented by steady diffusion flamelets, is parametrized. In the temperature-mixture fraction diagram, this zone is situated underneath the 'critical' flamelet, corresponding to the critical scalar dissipation rate at which extinction occurs. As mentioned before, the REDIM includes an 'underlying' scalar dissipation rate $\chi^\star$. In our case, in the zone above the critical flamelet, the scalar gradients that need to be specified in order to build the REDIM are obtained from steady laminar diffusion flamelets. In the low temperature region, the scalar gradients $\nabla\phi_\alpha^{(c)}$ from the 'critical flamelet' are specified, such that $\chi^\star = 2D\nabla Z^{(c)}.\nabla Z^{(c)}$, where D depends on (Z, Y_{CO_2}).

3.3. A Priori test of the REDIM

Before discussing the transported PDF calculations, the intrinsic potential of the 2D REDIM to reproduce experimentally measured values is tested

in compositional space. For a given Y_{CO_2} value (or Z value), scatter plots of the experimental measurements from all the axial positions are compared with the REDIM. A slice is taken from the REDIM at the specified Y_{CO_2} value (resp. Z value) and all the experimental measurements for $Y_{CO_2} \pm 0.02 Y_{CO_2}$ (resp. $Z \pm 0.02 Z$) are plotted. This 2% relative margin is somewhat arbitrary and accounts for experimental uncertainty.

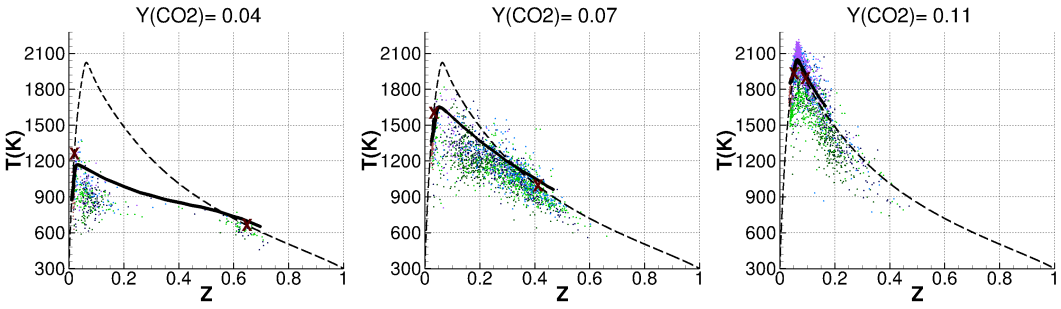

Figure 4: A Priori test: Temperature for constant values of Y_{CO_2}. Experimental measurements (dots), REDIM (full line) and reference steady non-premixed flamelet (dashed line and crosses).

In Figure 4 the temperature for constant values of Y_{CO_2} is plotted. The REDIM is able to follow the experimental measurements along with the reaction progress, albeit that the temperature is too high, especially for low Y_{CO_2}-values. This is in line with [47] where it was reported that temperatures tend to be over-predicted by the Warnatz mechanism due to early onset of combustion. For comparison, a reference steady non-premixed flamelet is plotted in Figure 4 as a dotted line. The two points on the flamelet corresponding to the given constant Y_{CO_2} value are marked as 'X'. This steady flamelet was calculated in the opposed-flow configuration with strain rate 100s^{-1} using the Warnatz mechanism [43] (intermediate between the upper REDIM boundary and the critical flamelet shown in Figure 2).

In Figure 5 the temperature for constant values of Z is plotted. The reference steady flamelet is also represented as a dotted line in this Y_{CO_2}-temperature space (and the flamelet value corresponding to the considered Z value is marked as 'X'). For all mixture fractions, the REDIM provides higher temperatures than what is experimentally measured. This is particularly true for low values of Y_{CO_2}, as already mentioned. Differences to the experimentally measured mean temperature are typically around 10%, but in specific regions they go up to 25%. This will result in over-prediction of

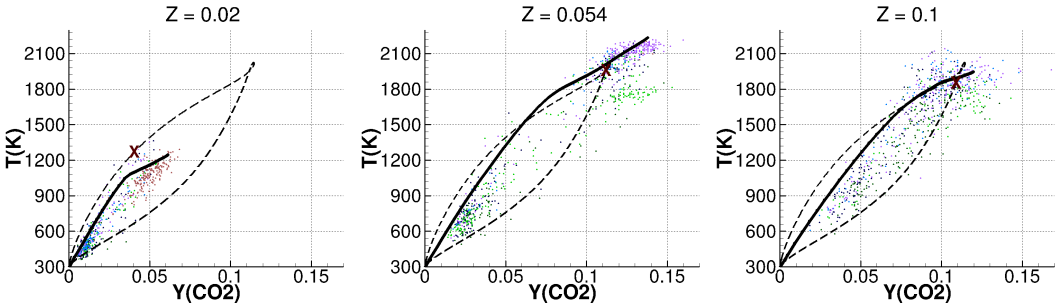

Figure 5: A Priori test: Temperature for constant values of Z. Experimental measurements (dots), REDIM (full line) and reference steady non-premixed flamelet for strain rate 100s^{-1} (dashed line and cross).

the mean temperature in the simulations discussed below.

The substantial amount of scatter around the REDIM seems to suggest that with a 3D REDIM more of the compositional space would be accessed, as in the experimental measurements. However, this scatter is certainly partly due to the experimental uncertainty [15]. In [48] the required dimension of the REDIM for a good representation of the kinetics is investigated, and there it is concluded that a 2D or 3D REDIM is optimal for CFD calculations. This is confirmed by the a priori study: the overall quality of the REDIM is deemed satisfactory for the modeling of the specific swirling flame considered.

4. Results

4.1. Flow and mixing fields (physical space)

We discuss here the mean velocity and scalar profiles obtained in physical space corresponding to the transported scalar PDF calculation using REDIM and EMST ('REDIM-EMST') with the ad hoc adjustment of the turbulent Schmidt number Sc_T described in Appendix A. The latter is necessary in order to capture the mean mixture fraction plateau in the region above the bluff body, and in order to correctly model the mixing of pure air with burnt products in the recirculation zone when using REDIM (the 'mixing line' in composition space discussed in the next section). In addition to the REDIM-EMST calculation, two calculations with a fast chemistry model are also considered: a presumed-PDF calculation ('Fastchem-β-PDF') and a transported scalar PDF with the same settings as the REDIM calculation ('Fastchem-EMST'). These calculations are included in order to show the

impact of the 'mixing line' on the results in physical space (since with the adjusted Sc_T, this 'mixing line' is indeed captured with REDIM and not with the fast chemistry that always leads to a burning solution). As 'fast chemistry' model, the single steady laminar flamelet with strain rate of 100s^{-1} is used (the dashed line represented in Figure 4).

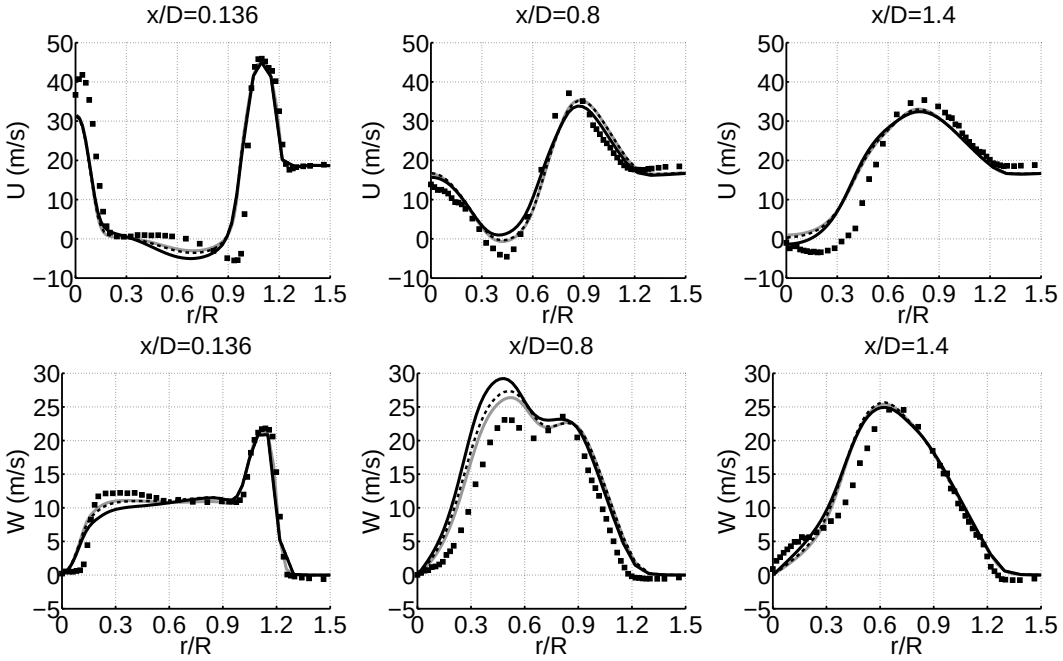

Figure 6: Mean axial and tangential velocity profiles. Grey line: Fastchem-β-PDF, Dashed black line: Fastchem-EMST, Full black line: REDIM-EMST, Symbols: experimental data.

Figure 6 reports the mean axial velocity $\widetilde{U}$. At $x/D = 0.136$, $\widetilde{U}$ is under-predicted by all calculations on the center line. The radial position of the first recirculation zone is not correctly predicted, but in the REDIM calculation the absolute value of the negative velocity is correct. At $x/D = 0.8$, the axial velocity in the center region is slightly over-predicted by all the calculations. The results show (almost) no small negative axial velocities. In the experiments, however, an area of negative velocities is still observed, indicating that the length of the first recirculation zone is under-predicted by all calculations. For all calculations, the width of the recirculation zone is smaller than in the experiments, but the axial position of the beginning of the second recirculation zone is reasonably predicted. The predictions

of the mean tangential velocity $\widetilde{W}$ are also satisfactory. At $x/D = 0.136$, the sharp gradient around $r/R = 0.15$ could not be captured by any of the calculations. The difference between Fastchem-EMST and REDIM-EMST results is the largest at $x/D = 0.8$, with all calculations over-predicting the experimental mean tangential velocity. Further downstream all the calculations correctly predict the tangential velocity. In general, agreement with experimental data is quite good, comparable to what was obtained with LES in [20]. As already observed in similar simulations of the non-swirling Sydney bluff-body flames [27, 28], the differences in mean density between the three different calculations do not strongly affect the mean flow field.

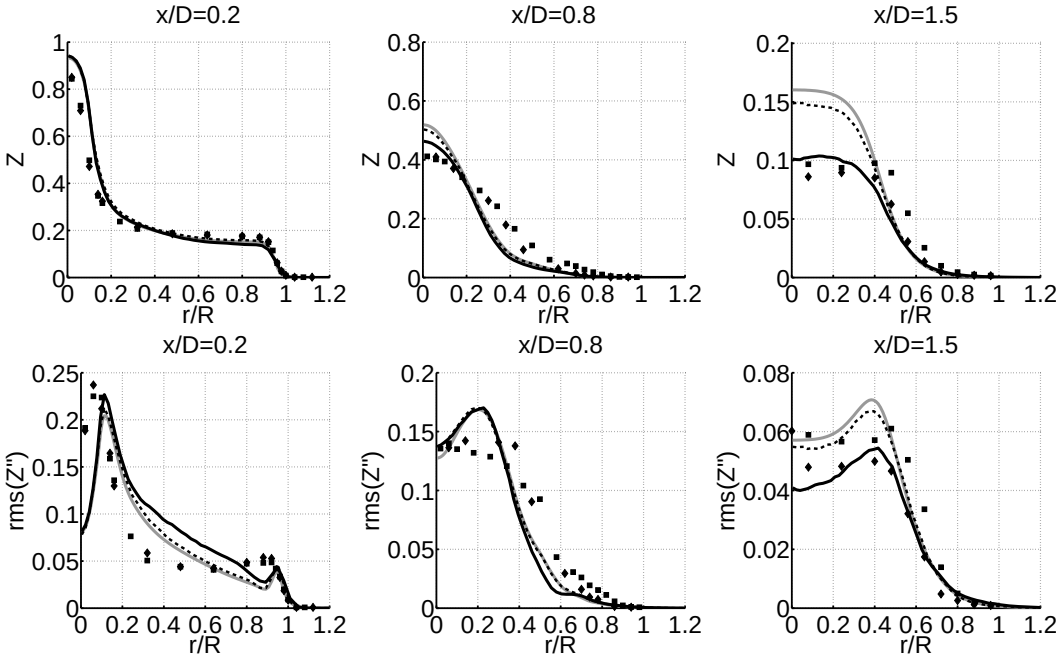

Figure 7: Mean mixture fraction and mixture fraction rms profiles. Grey line: Fastchem-β-PDF, Dashed black line: Fastchem-EMST, Full black line: REDIM-EMST, Symbols: experimental data.

In Figure 7 the mean mixture fraction and mixture fraction rms profiles are shown. At $x/D = 0.2$, the plateau in the bluff-body region and the steep gradient in the annulus region ($0.9 < r/R < 1.1$) have to be well predicted, as these regions are close to stoichiometry and therefore will strongly affect the flame. This is the reason for the choice of the variable Sc_T depending on $\widetilde{uv}$ (see Appendix A). The motivation for this ad hoc adjustment is that

good results for the mean mixture fraction field, particularly in the reaction region around $Z = 0.054$, are indispensable to discuss the influence of the tabulated chemistry on the results.

As can be observed in Figure 7, the REDIM-EMST calculation leads to overall good results. It is quite remarkable that, whereas the mean velocity results are similar for the three calculations, the mean mixture fraction results differ quite strongly, especially at $x/D = 1.5$. Such differences are not observed when using the standard value $Sc_T = 0.7$ (not shown), and neither were they observed in the non-swirling bluff-body flame calculations [27, 28] where a standard constant value for Sc_T was used. In these cases, the REDIM calculations do not correctly reproduce the mixing between pure air and hot products in the recirculation zone (no 'mixing line') and mainly lead to a burning solution similar to a single diffusion flamelet. The possible differences in mean density are then not strong enough to affect the mean mixture fraction field. In the present case, however, the difference in mean density is larger, and moreover, the decrease of the relative importance of turbulent diffusion on mean mixture fraction compared to convective terms (through the increase of Sc_T) makes the evolution of mean mixture fraction more sensitive to differences in mean density. These differences in mean density between REDIM and Fastchem calculations are strongly related to the use of the progress variable Y_{CO_2} in REDIM, as will be discussed in the next section, and can be indirectly observed in Figure 8 showing the profiles of mean CO_2 mass fraction $\widetilde{Y}_{CO_2}$ (since the mean density mainly depends on the mean temperature, which is in this case strongly correlated to $\widetilde{Y}_{CO_2}$).

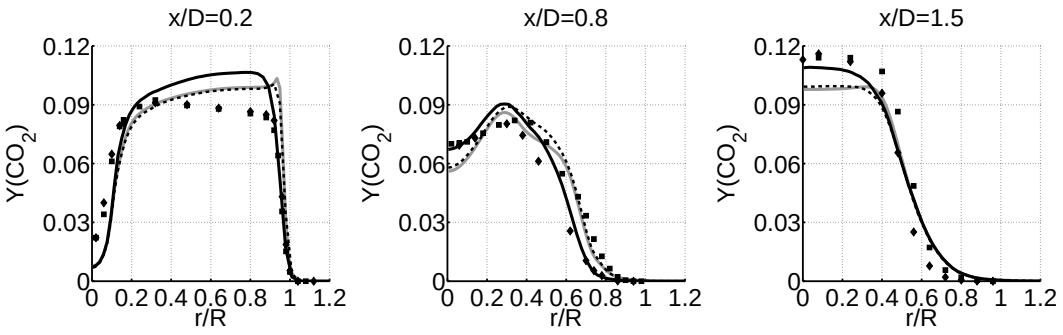

Figure 8: Mean Y_{CO_2} profiles. Grey line: Fastchem-β-PDF, Dashed black line: Fastchem-EMST, Full black line: REDIM-EMST, Symbols: experimental data.

4.2. Joint scalar PDF (composition space)

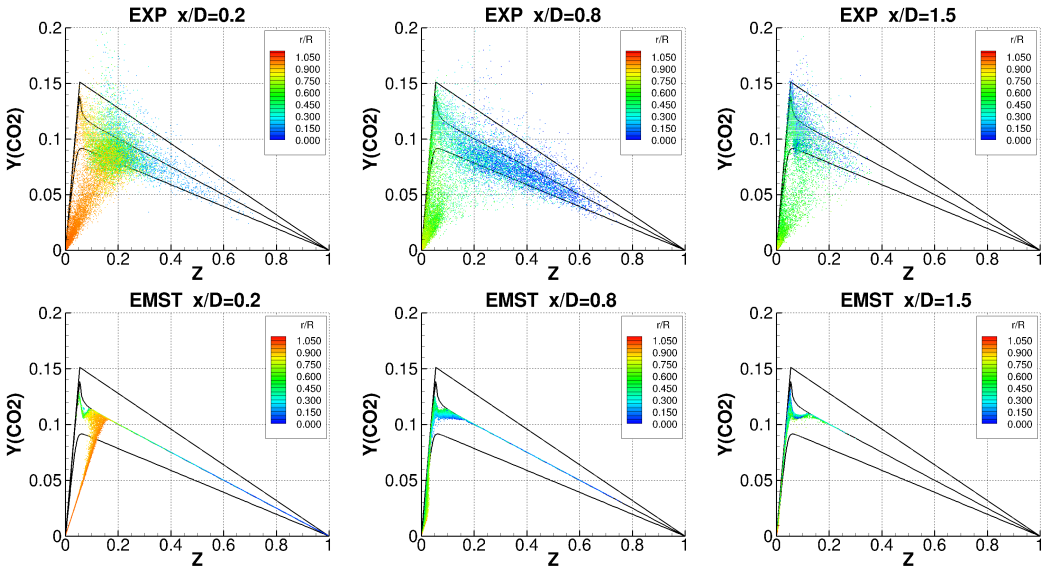

Figure 9: Scatter plots of Y_{CO_2} for experiments and REDIM-EMST calculation colored with r/R. The Burke-Schumann flame sheet (upper black line), upper boundary of the REDIM (middle black line) and the critical flamelet (lower black line) are also shown.

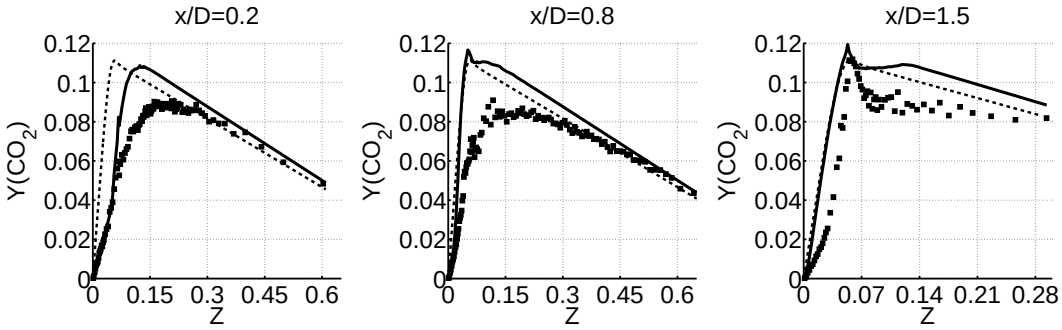

Figure 10: Conditional mean of Y_{CO_2}: Dashed black line: Fastchem-EMST, Full black line: REDIM-EMST, Symbols: experimental data.

Figure 9 shows the scatter plots of Y_{CO_2}, experimentally observed and numerically simulated. More quantitative information is given in Figure 10 showing the corresponding profiles for the conditional mean of Y_{CO_2}. Obviously, using the reference steady laminar flamelet (as 'fast chemistry model'),

all points would lie on this single laminar flamelet, as can be observed in Figure 10. With REDIM, a deviation from the single laminar flamelet is observed because Y_{CO_2} is a second independent parameter that enables to represent mixing of unburnt and burnt gases, different from the mixing in the laminar steady non-premixed flamelet.

However, hardly any scatter is observed, as expected in our RANS-EMST framework. On the one hand, the use of RANS may not permit to capture some large scale intermittency. On the other hand, and more importantly, the EMST mixing model which uses a mixing time scale proportional to the integral turbulent time scale, has limitations to model high scalar dissipation rate events [7, 8] as will be discussed below when introducing Equation (4).

In [13], local extinction and a mixing asymptote in the experimental results in compositional space are reported. In Figure 9 the latter can be recognized in the experimental scatter plot at $x/D = 0.2$ as the clustering of points around a line starting in the left bottom corner. This line, which is most likely due to mixing of burnt and unburnt gases in the shear layer between the annulus air flow and the recirculation zone close to the bluff body, is reproduced in the REDIM calculation with EMST as mixing model (and in [49], also with the modified Curl's mixing model [50]). This mixing line was also observed in [51], for the bluff-body flame HM1, which also has a recirculation zone caused by the bluff body. As shown in Figure 10, we can then correctly predict the conditional mean of Y_{CO_2} for lean mixtures at $x/D = 0.2$, although the cluster of experimental data around the laminar flamelet line observed in Figure 9 is missed. However, for rich mixtures between stoichiometry and $Z \approx 0.3$, the conditional mean is overestimated, due to the lack of scatter in the results.

At $x/D = 0.2$, for richer mixtures ($Z > 0.3$), we observe no scatter and all computational particles get their composition from the REDIM upper boundary. This could simply reflect the general limitations of our RANS-EMST modeling framework discussed above. It could also be explained by heat loss to the burner which is not taken into account, as discussed by Ihme et al. [52] for another swirling flame (SMH1). In Figure 9, the scatter plots are colored by the radial position in order to represent some correlation between composition and physical space. In the next section, the correlation between the scatter plots in composition space and the positions in physical space will help to better visualize how this rich branch in the modeled flame corresponds to a region located above the bluff body, consistent with the hypothesis of neglected heat loss of [52]. Note that in the experimental data

the scatter, which is not reproduced in our modeling approach, is observed both above and below the REDIM upper boundary, so that we still have good agreement for the conditional means. At $x/D = 0.8$ and 1.5, the REDIM-EMST scatter plots resemble a single diffusion flamelet, while the experimental scatter plots show a large amount of scatter below the 'critical flamelet', which is reflected in an over-prediction of the conditional mean of Y_{CO_2} in the simulations (Figure 10). This suggests that at these locations the REDIM-EMST calculation cannot capture the local extinction observed in the experiments and this will be discussed further in the next section, based on trajectories of computational particles.

5. Tracer trajectories

5.1. Characteristic regions in composition space

Following representative trajectories of particles is useful in order to discuss the correlation between the trajectories in physical space and the scatter plots in (Z, Y_{CO_2}) space. In order to correlate the trajectories in physical and composition space, we divided our (Z, Y_{CO_2}) space in different regions as shown in Figure 11a. These regions are delimited by the reference lines shown in Figure 2. Above the critical flamelet, we distinguish four zones: a lean region (dark blue), a stoichiometric region (yellow), a moderately rich region (green) and a rich region (brown). Below the critical flamelet, we make a distinction between a 'mixing line' region (light blue on the lean side, and dark purple on the rich side) and an intermediate region (red).

The critical flamelet is used in the DNS study of [5] in order to distinguish between a continuously burning region and a region where extinction and re-ignition occurs. In [5], not all points below the critical flamelet are interpreted as local extinction. Only particles coming from the flame zone and moving below the critical temperature profile are marked as extinguished. The history of the particle is clearly important. From Figure 2, we see that in the REDIM the critical flamelet goes through the region of highest CO_2 reaction rates. We can clearly see that the intermediate red region below the critical flamelet corresponds to a region of high CO_2 reaction rate such that this region will be modeled as a reaction zone (causing an upward motion in (Z, Y_{CO_2})-space). In order to possibly model extinction in this region of composition space, the mixing model should 'drive particles downwards' faster than the 'upwards motion' due to reaction. We would need a short mixing time compared to the reaction time (inverse of reaction rate) along

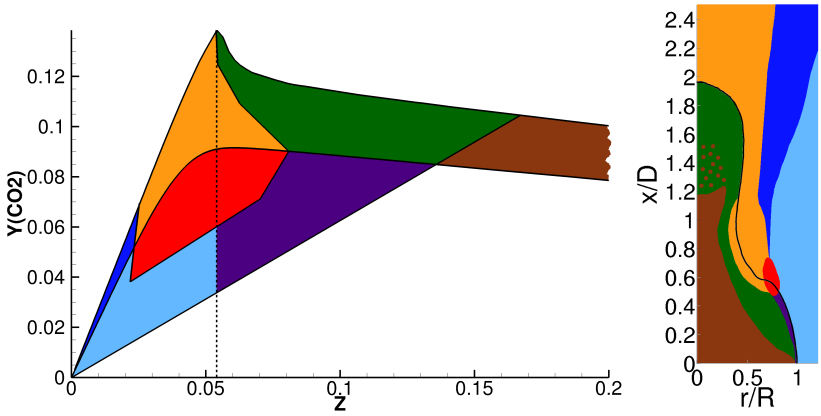

Figure 11: a/ Characteristic regions in composition space (left). b/ Map of the corresponding regions of the modeled flame in physical space (right).

the Y_{CO_2} direction in composition space. This mixing time can be written $1/\chi^*_{CO_2}$, where we can expect the modeled scalar dissipation rate for Y_{CO_2} to be of the IEM-type when using the EMST mixing model:

$$\chi^*_{CO_2} = C_\phi \omega^* \left(Y^*_{CO_2} - \widetilde{Y_{CO_2}} \right)^2 \quad \text{with} \quad \omega^* = \frac{\epsilon}{k}. \tag{4}$$

This scalar dissipation rate will be large if both the particle turbulence frequency ω^* and the particle Y_{CO_2}-fluctuation squared are large. However, the use of a mean turbulence frequency ϵ/k in the EMST mixing model implies a strong limitation in order to model high $\chi^*_{CO_2}$ events. A mixing model based on a scalar dissipation rate of the form of Equation (4) including a modeled fluctuating turbulence frequency ω^* like the PSP mixing model [7–10] could provide a better framework in order to model local extinction.

We can therefore expect that it will be difficult to model local extinction below the critical flamelet with our modeling approach. Following particle trajectories will be useful in order to distinguish between local extinction and mixing, and to better understand the capacities and limitations of our modeling approach.

5.2. Map of characteristic regions of the modeled flame in physical space

Figure 11b shows a general map of the different characteristic zones of the modeled flame in physical space. It provides a general qualitative correlation between the different regions of composition space represented in Figure 11a

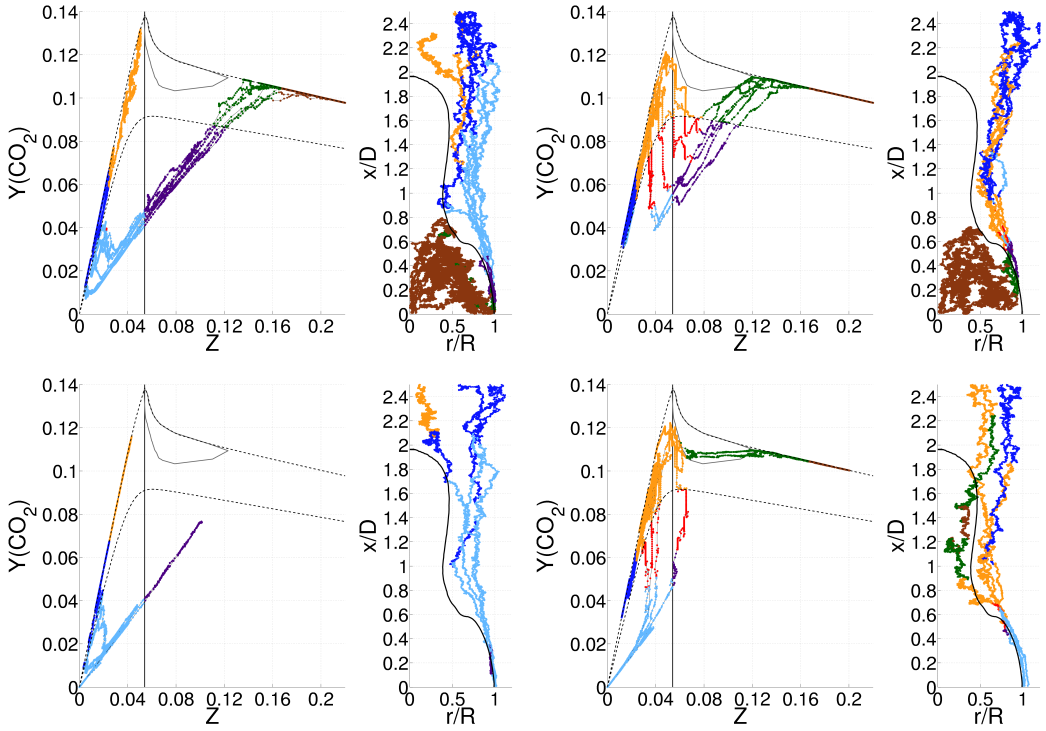

Figure 12: Trajectories of tracers interacting with the first recirculation zone. Tracers injected in the fuel jet: a/ without reaction and b/ reacting at the tip of the first recirculation zone. Tracers injected in the air coflow: c/ without reaction and d/ reacting at the tip of the first recirculation zone. Colour legend: see Figure 11

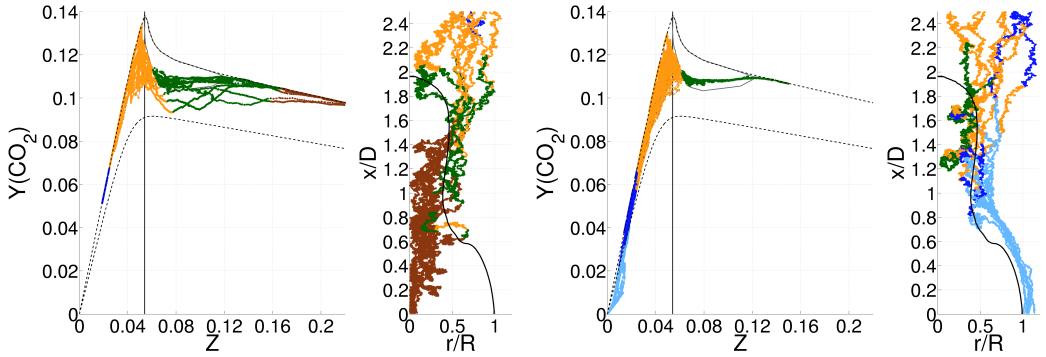

Figure 13: Trajectories of tracers passing around the first recirculation zone: a/ tracers injected in the fuel jet and b/ tracers injected in the air coflow. Color legend: see Figure 11

and the positions in physical space. This map was drawn by looking at a large number of tracer trajectories as shown in Figures 12 and 13. Note that from the scatter plots shown in Figure 9, we could already identify that the mixing line observed in the scatter plots corresponds to the mixing of burnt and unburnt gases in the shear layer at the edge of the outer recirculation zone (light blue and dark purple regions), or that the rich flamelet branch corresponds to the inner recirculation zone (brown region). On the other hand, the tracer trajectories help to show that ignition occurs at the tip of the outer recirculation zone (red region). A more detailed discussion of representative tracer trajectories will now permit to show that our modeling approach cannot capture local extinction in the highly rotating collar region, and we will see that the second recirculation zone (where re-ignition is observed experimentally) is modeled as a rich hot zone.

5.3. Trajectories in the outer edge of the first recirculation (mixing line)

Fuel and air tracers may have trajectories in the outer edge of the first recirculation zone as shown in Figure 12, where the fuel tracers have to cross the first recirculation zone, while the air tracers are directly injected at the outer edge. While crossing the first recirculation zone, the fuel tracers mix in the outer vortex with recirculated combustion products, resulting in an evolution towards stoichiometry along the rich flamelet branch. Eventually this hot (high Y_{CO_2}) rich mixture, mixes with air in the outer edge of the first recirculation zone. This mechanism of heating up the rich mixture before it mixes with fresh air stabilizes the flame and it is a direct result of the recirculation zone caused by the bluff-body. Depending on the trajectory in physical space, the particles fully mix in (Z, Y_{CO_2}) space towards the origin (as in Figure 12a) or deviate from the mixing line due to reaction (as in Figure 12b), and similar observations can be made for tracers injected in the air coflow.

Such representative trajectories of single tracers are shown in Figures 14 and 15 and will now be discussed in more detail. Note that after interaction in the shear layer between the outer vortex and the annulus air flow, a part of the particles recirculate in the outer vortex. These more complex recirculating trajectories can easily be interpreted as combinations of simpler trajectories. Therefore, in order to make the discussion easier, we choose to focus on simple trajectories that provide the essential information. A more detailed study of the tracers can be found in [53].

5.3.1. Mixing line: no reaction at the tip of the recirculation zone

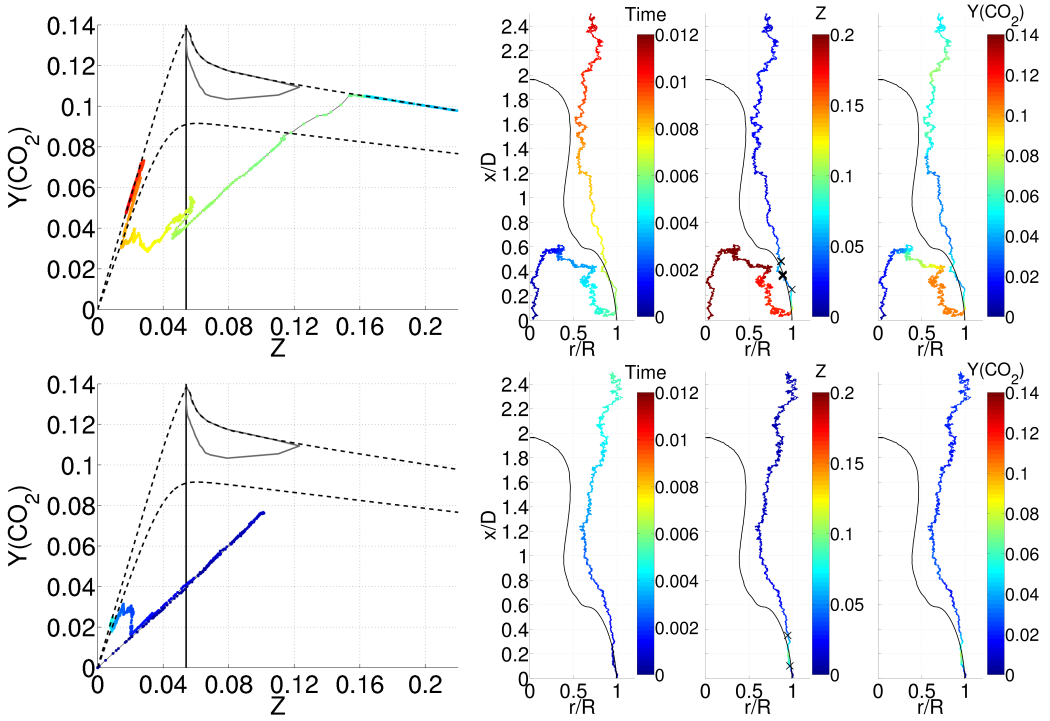

Figure 14: Representative trajectories of tracers interacting with the outer edge of the first recirculation zone without reaction (top: injected in the fuel jet / bottom: injected in the air coflow). Left: evolution in (Z, Y_{CO_2}) space colored by time. Right: evolution in physical space colored by time, Z (color-scale clipped at $Z = 0.2$, crosses: Z_{st}) and Y_{CO_2}. Black line: mean stoichiometric mixture fraction line.

Figure 14 reveals that the representative fuel tracer is first picked up by the inner vortex and passed on to the outer vortex in the first recirculation zone. During this period in time, the particle evolves in composition space along the rich flamelet branch. Once the annulus region is reached, the particle starts to mix with fresh air, represented in composition space by a mixing line almost straight from the point where the particle leaves the rich flamelet branch towards the origin $(0, 0)$. Evolution along this mixing line brings the particle below the 'critical flamelet' but this is no local extinction as the particle was not burning during or prior to its evolution along the mixing line. For this specific tracer there is a deviation from this mixing line, around stoichiometry: the tracer evolves to higher Y_{CO_2} and Z values, due to mixing with rich combustion products. Eventually the particle moves

horizontally in composition space to the lean flamelet branch, along which it evolves upwards, due to mixing with combustion products. Finally, it evolves downward, along the lean flamelet branch due to mixing with leaner gases.

Similar observations can be made for the air tracer. We mainly observe mixing between fresh air and hot products, and Y_{CO_2} remains low enough such that those tracers do not enter the region of high reactivity (i.e. it does not enter the red region in composition space in Figure 11).

5.3.2. Mixing line: reaction at the tip of the recirculation zone

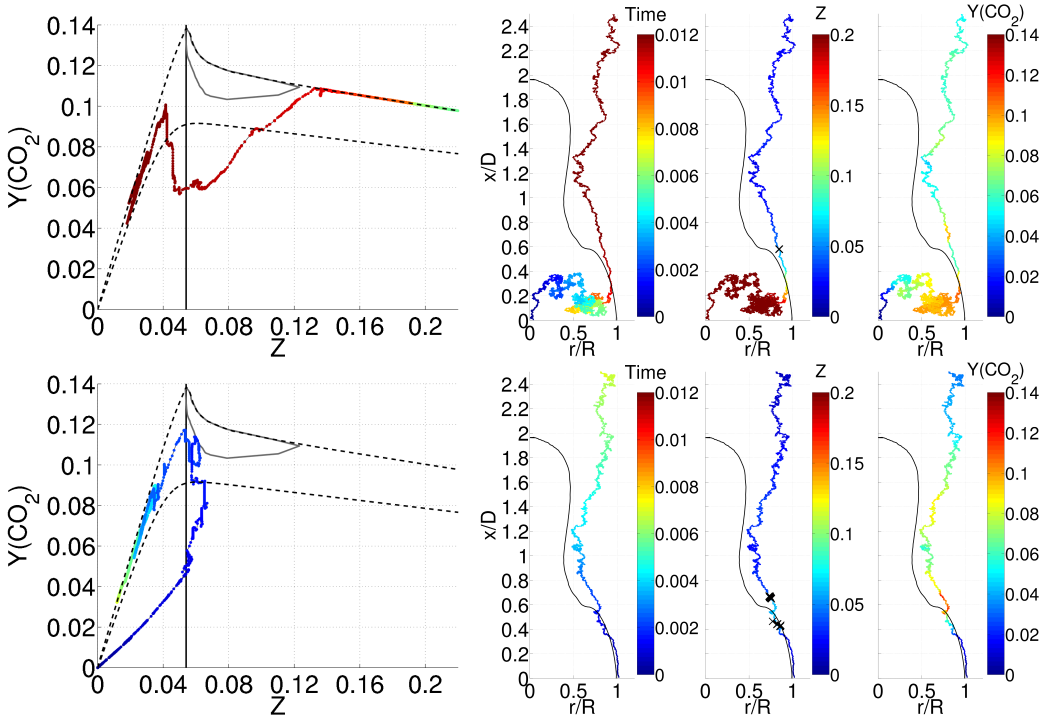

Figure 15: Representative trajectories of tracers interacting with the outer edge of the first recirculation zone and reacting at the tip of the recirculation zone (top: injected in the fuel jet / bottom: injected in the air coflow). Legend: see Figure 14.

Figure 15 shows tracer trajectories with an upward motion in Y_{CO_2}-space, also observed as a steep increase of Y_{CO_2} in physical space at the tip of the first recirculation zone, where the tracer enters the red zone of high reactivity in composition space (Figure 11).

The representative fuel tracer first moves away horizontally from the mixing line, before reacting. The tracer evolves in a stepwise sense to the

lean flamelet branch, intermittently switching between reaction (vertical) and mixing (sideward). Downstream interaction with air corresponds to an evolution along the lean flamelet branch. Similar trajectories were shown in Figure 12b. Along these trajectories there are small downward movements in the red and yellow zone in (Z, Y_{CO_2}) space, indicating that mixing may compete with reaction in the region of high reactivity, which corresponds to the highly rotating collar zone in physical space. These are relatively rare events causing only a small downward movement in (Z, Y_{CO_2}) space compared to the upward movements due to reaction. In general, no local extinction is observed for these tracers.

5.4. Trajectories passing around the first recirculation

5.4.1. Fuel particles crossing the neck zone

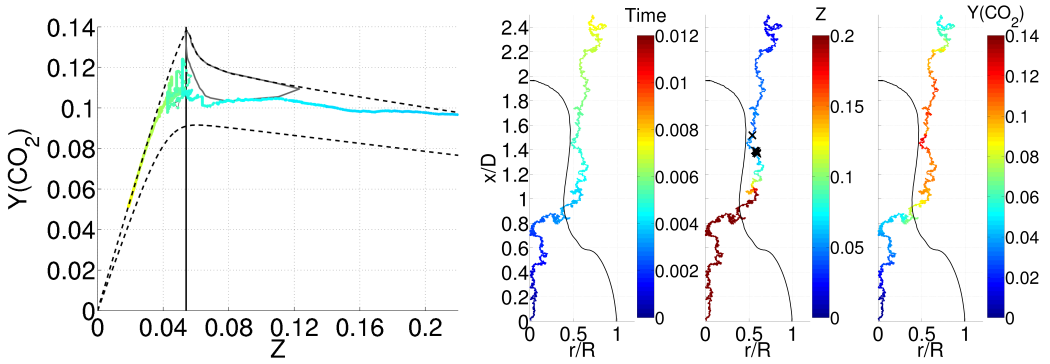

Figure 16: Representative trajectory of a fuel tracer not crossing through the first recirculation zone. Legend: see Figure 14.

Figure 16 shows a tracer trajectory that resembles a non-premixed flamelet in composition space and a jet-like trajectory in physical space. The particle flows past the first recirculation zone, meanwhile interacting with the inner vortex. In composition space this corresponds to an evolution along the rich flamelet branch. Downstream of the first recirculation zone the particle becomes stoichiometric towards the outer side of the second recirculation zone. There, around stoichiometry, there is much alternating vertically upward (reaction), downward and sideward (mixing) evolution in composition space. Note that this corresponds to the end of the highly rotating collar region. As observed in the previous section, in the upstream part of the highly rotating collar region, we may say that mixing competes with reaction, but not

enough in order to model local extinction. Further downstream the particle interacts with air, in composition space corresponding to an evolution along the lean flamelet branch.

5.4.2. Air particles interacting with the second recirculation zone

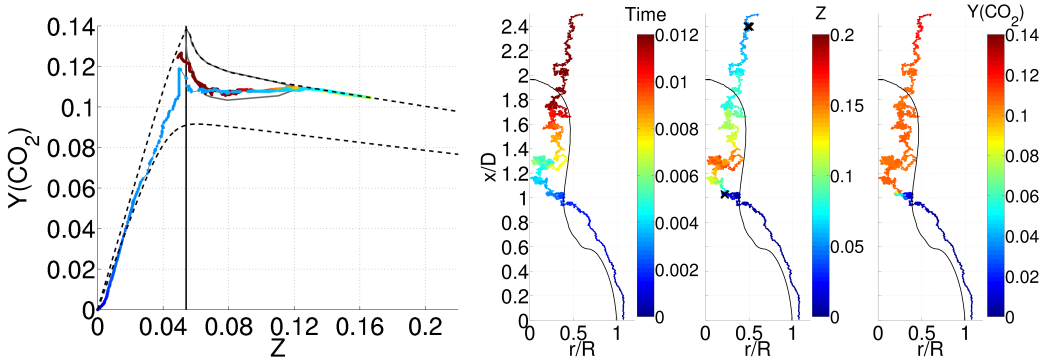

Figure 17: Representative trajectory of an air tracer interacting with the second recirculation zone. Legend: see Figure 14.

The representative tracer shown in Figure 17 first follows very briefly a mixing line, but very quickly evolves upward in composition space along a lean flamelet branch. Interaction with reacting particles thus appears in composition space as a flamelet-like evolution. Crossing stoichiometry, reaction takes place. In the rich region, which corresponds to the second recirculation zone in physical space, mixing with rich hot products takes place, seen as horizontal paths in composition space. This is in agreement with the experimental observation that the re-circulated hot products from the second recirculation zone would cause re-ignition.

6. Conclusions

Steady axisymmetric transported scalar PDF modeling of a swirling flame stabilized behind a bluff-body burner (swirling flame 'SM1') with a 2D Reaction Diffusion Manifold (REDIM) has been discussed. With an ad hoc adjustment of the turbulent Schmidt number, the results in physical space for flow and mixing fields, obtained in a non-linear k-ϵ RANS modeling framework, are in reasonable agreement with experimental data and comparable to LES results from the literature.

In REDIM, the concept of progress variable is used — in the present case the CO_2 mass fraction Y_{CO_2} — and the entire (Z, Y_{CO_2}) space is covered. An a priori study has been performed, indicating that the REDIM can capture the main features of the experimental measurements in (Z, Y_{CO_2}) space. Compared to a modeling based on a single steady laminar flamelet (which can be seen as a fast chemistry model in the 1D Z-space), results obtained with REDIM for the turbulent flow, temperature and composition fields are in general in better agreement with experimental data in physical space. This is related to the modeling in composition space, where the REDIM benefits from the use of a progress variable, allowing access to the low Y_{CO_2}-region. As a result, the mixing between fresh air and hot products in the recirculation zone above the bluff-body burner can be modeled.

This important qualitative agreement is observed in the (Z, Y_{CO_2}) scatter plots, as a mixing line in composition space. This mixing line, also observed in the non-swirling bluff-body flames, is indeed due to mixing between fresh air and hot products and not due to local extinction. On the other hand, the calculation results represent too little scatter compared to the experimental data, especially downstream. This indicates that the local extinction which is assumed to occur experimentally in the highly rotating collar region is not captured in the present modeling framework. The fact that heat loss at the bluff-body surface is neglected, as discussed by Ihme et al. [52] for another swirling flame, also appears to be a plausible explanation for the underestimation of scatter on the rich side.

The trajectories of computational particles in composition space and physical space have been studied as these allow to distinguish mixing from local extinction, which is not possible by means of local scatter plots alone. Through analysis of the trajectories, we can also better understand the correlation between the scatter plots in composition space and the positions in physical space. After defining some characteristic zones in composition space, we could sketch a corresponding map in physical space, by looking at a large number of tracer trajectories.

The trajectories confirm the hypothesis of the mixing of particles with different reaction progress in the annulus region close to the bluff body, resulting in a mixing line in composition space. This illustrates how mixing of fresh air with hot products in the first recirculation zone — the main mechanism that stabilizes the bluff-body flames (swirling and non-swirling) — is modeled in this transported scalar PDF modeling approach. Local extinction, in the sense of initially burning particles moving in composition space into a

region below the critical flamelet, has not been observed in the simulations. However, in (Z, Y_{CO_2}) space some small downward movements have been observed in the zones of high reactivity, corresponding to the highly rotating collar region in physical space. This indicates that we are able to capture the competition between mixing and reaction in this region of physical space, but not enough in order to model local extinction. This can be attributed to the limitation of modeling high Y_{CO_2} scalar dissipation rate events when using the EMST mixing model based on the mean integral turbulent time scale. Finally, the trajectories show how the second recirculation zone is modeled as a hot region of rich combustion products, in agreement with experimental observations.

Acknowledgements

This collaborative research is supported by the Comunidad de Madrid through Project HYSYCOMB P2009/ENE-1597 and by the Spanish Ministry of Science and Innovation under Projects ENE2008-06515-C04-02 and CSD2010-00011.

Furthermore this work is funded by the Special Research Fund of Ghent University under project BOF07/DOC/210.

Appendix A. Turbulent Schmidt number

The motivation for the use of a variable turbulent Schmidt number Sc_T stems from an observation of experimental data and calculation results obtained using a constant Sc_T.

In Figure A.18, we observe a plateau above the bluff body for mean mixture fraction (with a value close to $\widetilde{Z} = 0.2$) in the first radial profiles at $x/D = 0.2$. This plateau is missed in our non-linear k-ϵ calculation, where the turbulent flux for mean mixture fraction is modeled using a gradient diffusion model with a constant turbulent Schmidt number with standard value $Sc_T = 0.7$. We could say that we model "too much turbulent diffusion" on the outer edge of the recirculation zone. A first idea would then be to lower the diffusion coefficient by increasing the turbulent Schmidt number. We can see that results obtained with a higher constant value $Sc_T = 1.5$ are indeed improved close to the bluff body, allowing to capture the plateau. However, we observe that further downstream, mean mixture fraction is overestimated on the center-line.

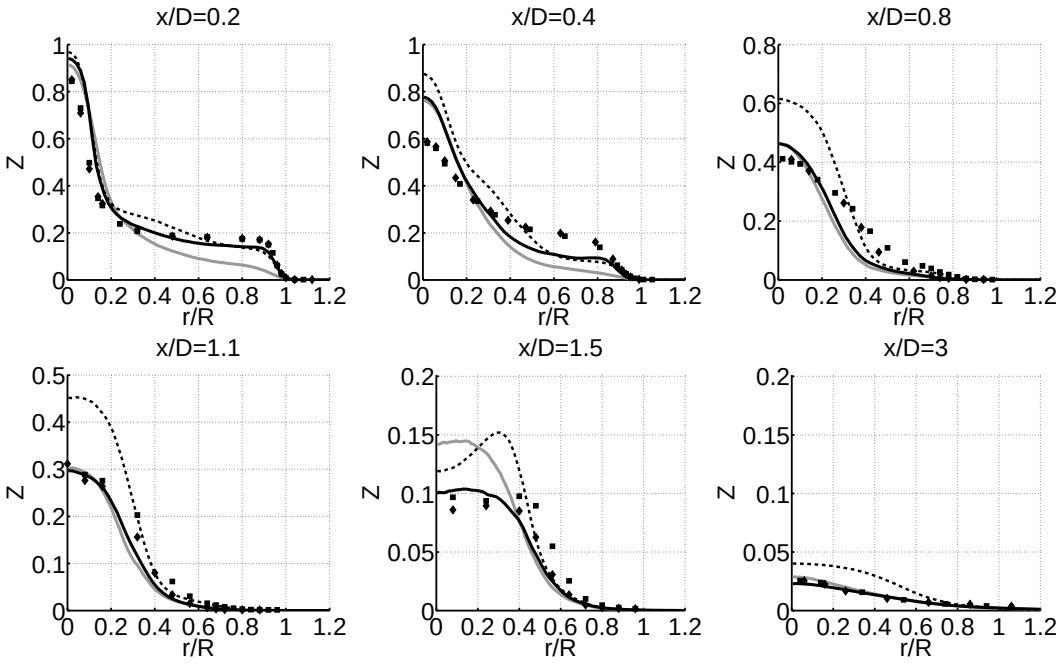

Figure A.18: Mean mixture fraction profiles from REDIM-EMST transported PDF calculations. Full black line: variable Sc_T. Dashed line: $Sc_T = 1.5$. Grey line: $Sc_T = 0.7$. Symbols: experimental data.

By looking at experimental results for mean mixture fraction in Figure A.18 and for mean axial velocity in Figure A.19, we can see that the steep gradients for mean mixture fraction (the edges of the plateau) coincide with the edges of the first recirculation zone. This observation is the basis for an ad hoc adjustment of the turbulent Schmidt number. The idea is to propose a variable Sc_T that will get the standard constant value $Sc_T = 0.7$ except in the zones corresponding to the edges of the first recirculation zone where it will locally get a higher value.

A way to characterize the edge of the recirculation zone is to look for the high values of the gradient of mean axial velocity $\widetilde{U}$ in the radial direction $\partial\widetilde{U}/\partial r$, or to look for the high values of the shear stress $\widetilde{uv}$ directly related to the velocity gradients in the algebraic model used here:

$$-\langle\rho\rangle\widetilde{uv} = \mu_T \left(\frac{\partial\widetilde{U}}{\partial r} + \frac{\partial\widetilde{V}}{\partial x} \right) \tag{A.1}$$

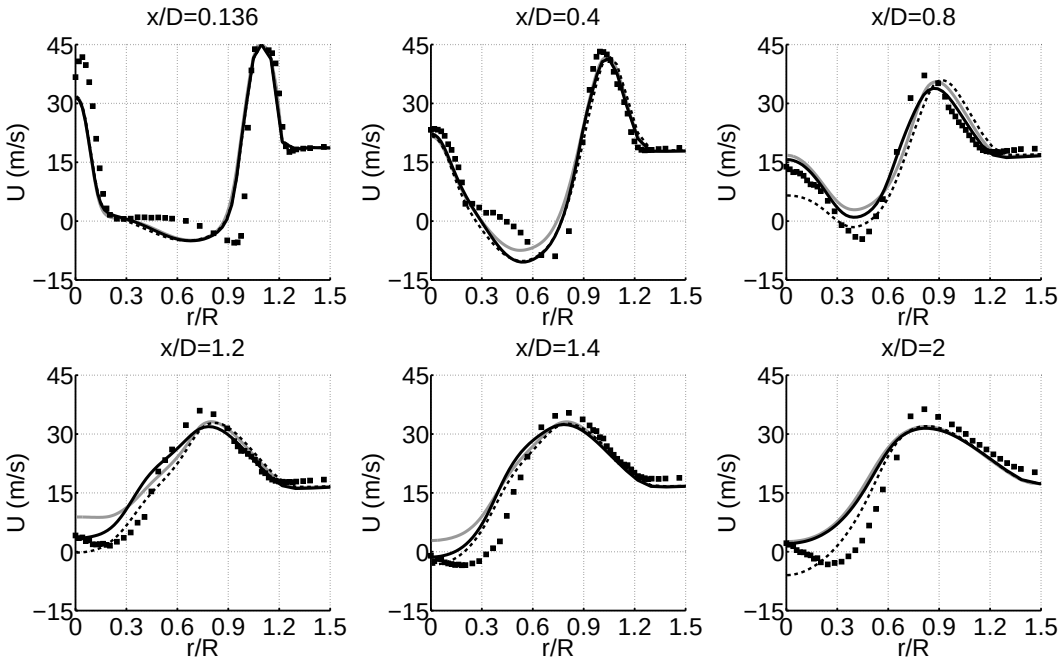

Figure A.19: Mean Axial Velocity profiles from REDIM-EMST transported PDF calculations. Full black line: variable Sc_T. Dashed line: $Sc_T = 1.5$. Grey line: $Sc_T = 0.7$. Symbols: experimental data.

The ad hoc adjustment proposed is based on the following factor:

$$\begin{aligned} \lambda &= -2\frac{\widetilde{uv}}{\sqrt{\widetilde{uu}.\widetilde{vv}}} \qquad \text{if} \quad \widetilde{uv} < \widetilde{uv}^{(-)}_{\text{thres}} \quad \text{or} \quad \widetilde{uv} > \widetilde{uv}^{(+)}_{\text{thres}} \\ \lambda &= 0 \quad \text{otherwise,} \end{aligned} \tag{A.2}$$

where $\lambda > 0$ corresponds to the outer edge of the recirculation zone (where $\widetilde{uv} < 0$), and $\lambda < 0$ corresponds to the inner edge. We used the threshold values $\widetilde{uv}^{(-)}_{\text{thres}} = -10$ and $\widetilde{uv}^{(+)}_{\text{thres}} = 20$ in order to localize the outer and inner edges respectively.

We moreover restrict ourselves in physical space to the zone above the bluff-body (with maximum axial coordinate X_{lim} and maximum radial coordinate R_{lim}) and introduce a smooth transition to zero in axial direction

(between $X_{\lim}/2$ and $X_{\lim}$):

$$\begin{aligned} \lambda^* &= \lambda.\frac{1}{2}\left\{1+\sin\left[\pi\left(\frac{x}{X_{\lim}/2}-\frac{1}{2}\right)\right]\right\} \qquad \text{if} \quad x < X_{\lim}, \quad r < R_{\lim} \\ \lambda^* &= 0 \quad \text{otherwise,} \end{aligned} \tag{A.3}$$

with $X_{\lim} = 0.05$ and $R_{\lim} = 0.03$.

We finally decide by how much the turbulent Schmidt number should locally be multiplied:

$$Sc_T = 0.7\,(1+\lambda^{**})\,, \tag{A.4}$$

where

$$\begin{aligned} \lambda^{**} &= \lambda^{(\text{inner})}\text{MIN}(1,-\lambda^*) \qquad \text{if} \quad \lambda^* < 0 \\ \lambda^{**} &= \lambda^{(\text{outer})}\text{MIN}(1,\lambda^*) \qquad \text{if} \quad \lambda^* > 0, \end{aligned} \tag{A.5}$$

with $\lambda^{(\text{inner})} = 1$ and $\lambda^{(\text{outer})} = 3$, such that Sc_T is at most multiplied by 2 on the inner edge and by 4 on the outer edge of the first recirculation zone.

Figure A.20 shows how the adjustment only affects a restricted zone of the computational domain (at the outer and inner edges of the first recirculation zone), while $Sc_T = 0.7$ almost everywhere.

References

[1] D. Veynante, L. Vervisch, Progres in Energy and Combustion Science 28 (2002) 193-266

[2] A. Yoshida, T. Igarashi, Y. Kotani, Combustion and Flame 109 (1997) 669-681

[3] S.K. Omar, D. Geyer, A. Dreizler, J. Janicka, Progress in Computational Fluid Dynamics 4 (3-5) (2004) 241-249

[4] F. Takahashi, V.R. Katta, Twenty-Sixth Symposium (International) on Combustion (1996) 1151-1160

[5] S. Mitarai, J.J. Riley, G. Kosaly, Physics of Fluids 15 (12) (2003) 3856-3866

[6] P. Sripakagorn, S. Mitarai, G. Kosaly, H. Pitsch, Journal of Fluid Mechanics 518 (2004) 231-259

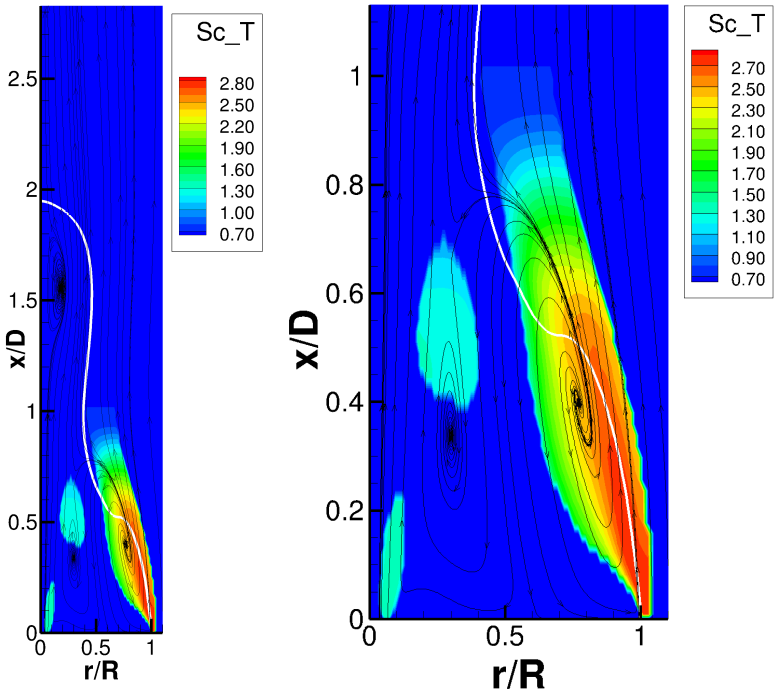

Figure A.20: Contours of Sc_T with streamlines: entire computational domain (left) and zoom on the first recirculation zone (right).

[7] D.W. Meyer, P. Jenny, Combustion and Flame, 155 (3) (2008) 490-508

[8] D.W. Meyer, P. Jenny, Proceedings of the Combustion Institute 32 (2009) 1613-1620

[9] D.W. Meyer, P. Jenny, Journal of Computational Physics 228 (2009) 1275-1293

[10] M. Hegetschweiler, B. Zoller, P. Jenny, Combustion and Flame (2011) in press

[11] M. Ihme and H. Pitsch, Combustion and Flame 155 (1-2) (2008) 90-107.

[12] J.A. van Oijen and L.P.H. de Goey, Combustion Science and Technology 161 (2000) 113-137.

[13] P.A.M. Kalt, Y.M. Al-Abdeli, A.R. Masri and R.S. Barlow, Proceedings of the Combustion Institute 29 (2003) 1913-1919.

[14] Y.M. Al-Abdeli and A.R. Masri, Experimental Thermal and Fluid Science 27 (5) (2003) 655-665.

[15] A.R. Masri, P.A.M. Kalt and R.S. Barlow, Combustion and Flame 137 (1-2) (2004) 1-37.

[16] Y.A. Al-Abdeli, A.R. Masri, G.R. Marquez and S.H. Starner, Combustion and Flame 146 (1-2) (2006) 200-214.

[17] A.R. Masri, P.A.M. Kalt, Y.M. Al-Abdeli and R.S. Barlow, Combustion Theory and Modelling 11 (5) (2007) 653-673.

[18] A.R. Masri, S.B. Pope and B.B. Dally, Proceedings of the Combustion Institute 28 (2000) 123-131.

[19] S. James, J. Zhu and M.S. Anand, Proceedings of the Combustion Institute 31 (2007) 1737-1745.

[20] A. Kempf, W. Malalasekera, K.K.J. Ranga-Dinesh and O. Stein, Flow Turbulence and Combustion 81 (4) (2008) 523-561.

[21] W. Malalasekera, K.K.J. Ranga-Dinesh, S.S. Ibrahim and A.R. Masri, Combustion Science and Technology 180 (5) (2008) 809-832.

[22] O. Stein and A. Kempf, Proceedings of the Combustion Institute 31 (2007) 1755-1763.

[23] H. El-Asrag and S. Menon, Proceedings of the Combustion Institute 31 (2007) 1747-1754.

[24] C. Olbricht, F. Hahn, A. Ketelheun, J. Janicka, Journal of Turbulence 11 (38) (2010) 1-18

[25] B. Merci and E. Dick, International Journal of Heat and Mass Transfer 46 (3) (2003) 469-480.

[26] V. Bykov and U. Maas, Combustion Theory and Modelling 11 (6) (2007) 839-862.

[27] B. Merci, B. Naud, D. Roekaerts and U. Maas, Flow Turbulence and Combustion 82 (2) (2009) 185-209.

[28] D. Roekaerts, B. Merci, B. Naud and U. Maas, International Journal for Multiscale Computational Engineering 7 (6) (2009) 487-508.

[29] S. Subramaniam and S.B. Pope, Combustion and Flame 115 (4) (1998) 487-514.

[30] in: http://www.aeromech.usyd.edu.au/thermofluids/swirl_files/burner-plan.pdf, (2002).

[31] S.B. Pope, Progress in Energy and Combustion Science 11 (2) (1985) 119-192.

[32] B. Naud, C. Jimenez and D. Roekaerts, Progress in Computational Fluid Dynamics 6 (1-3) (2006) 146-157.

[33] M. Muradoglu and S.B. Pope, Aiaa Journal 40 (9) (2002) 1755-1763.

[34] B.E. Launder, G.J. Reece and W. Rodi, Journal of Fluid Mechanics 68 (APR15) (1975) 537-566.

[35] G. Li,B. Naud and D. Roekaerts, Numerical investigation of a bluff-body stabilised nonpremixed flame with differential Reynolds-Stress models, Flow, Turbulence and Combustion 70 (2003) 211-240

[36] H. Wang, S.B. Pope, Combustion Theory and Modelling 12 (5) (2008) 857-882

[37] S.B. Pope, Combustion Theory and Modelling 1 (1) (1997) 41-63.

[38] L.Y. Lu, S.R. Lantz, Z.Y. Ren and S.B. Pope, Journal of Computational Physics 228 (15) (2009) 5490-5525.

[39] O. Gicquel, N. Darabiha and D. Thevenin, Proceedings of the Combustion Institute 28 (2000) 1901-1908.

[40] D.A. Goussis and U. Maas, in: Echekki T. and Mastorakos N. (Eds.), Turbulent Combustion Modeling: Advance, New Trends and Perspectives, Fluid Mechanics and Its Applications, Vol. 95, Springer-Verlag, 2011, p193-220.

[41] U. Maas and S.B. Pope, Combustion and Flame 88 (3-4) (1992) 239-264.

[42] A.E. Lutz, R.J. Kee, J.F. Grcar and F.M. Rupley, OPPDIF: a Fortran program for computing opposed-flow diffusion flames, Report No. SAND96-8243, Sandia National Laboratories, 1996.

[43] J. Warnatz, U. Maas and R.W. Dibble, Combustion physical and chemical fundamentals, modeling and simulation, experiments, pollutant formation, Springer, Berlin, 2006.

[44] M. Ihme and H. Pitsch, Combustion and Flame 155 (1-2) (2008) 70-89.

[45] C.D. Pierce and P. Moin, Journal of Fluid Mechanics 504 (2004) 73-97.

[46] K. Bray, P. Domingo and L. Vervisch, Combustion and Flame 141 (4) (2005) 431-437.

[47] H. Pitsch and H. Steiner, Physics of Fluids 12 (10) (2000) 2541-2554.

[48] K. Konig, V. Bykov and U. Maas, Flow Turbulence and Combustion 83 (1) (2009) 105-129.

[49] R. De Meester, B. Naud and B. Merci, Proceedings of the 7th Mediterranean Combustion Symposium (2011) (TC-21)

[50] J. Janicka, W. Kolbe and W. Kollmann, Journal of Non-Equilibrium Thermodynamics 4 (1) (1979) 47-66.

[51] K. Liu, S.B. Pope,D.A. Caughey, Combustion and Flame 141 (1-2) (2005) 89-117

[52] M. Ihme, C. Schmitt and H. Pitsch, Proceedings of the Combustion Institute 32 (2009) 1527-1535.

[53] R. De Meester, PhD thesis, Ghent University, 2012 (in preparation)